HOKKAIDO UNIVERSITY

Title	Study on the Simulation of the R.F.Corona Discharge in Nitrogen : F.C.T.SHASTA algorithm in the spheroidal coordinate system
Author(s)	Sato, Nobuyasu; Tagashira, Hiroaki
Citation	北海道大學工學部研究報告, 126, 21-34
Issue Date	1985-05-31
Doc URL	https://hdl.handle.net/2115/41935
Type	departmental bulletin paper
File Information	126_21-34.pdf

Hokkaido University Collection of Scholarly and Academic Papers : HUSCAP

北海道大学工学部研究報告
第126号（昭和60年）

Bulletin of the Faculty of Engineering,
Hokkaido University, No. 126 (1985)

Study on the Simulation of the R. F. Corona Discharge in Nitrogen.

—— F. C. T. SHASTA algorithm in the spheroidal coordinate system. —

Nobuyasu. SATO and Hiroaki. TAGASHIRA
Department of Electrical Engineering
(Received December 27, 1985)

Abstract

Computer simulation procedures for the r. f. corona discharge between a hyperboloidal needle and plane electrodes in nitrogen are outlined. The continuity equations for electrons, positive ions and excited molecules, and Poisson's equation are represented in the spheroidal coordinate system. The F. C. T. Phoenical L. P. E. SHASTA algorithm is used to solve the continuity equation for electrons. Boundary conditions are investigated by taking into account the space charge effects and geometrical factors of the secondary processes. A brief flow chart for the computation is given.

1. Introduction.

The development of the r. f. corona discharge between a hyperboloidal needle and plane electrodes in nitrogen has been investigated experimentally.[1] This experiment revealed distinctive characteristics of the r. f. corona development such as the polarity effect, hysteresis and progressive space charge accumulation process. The electrode configuration used in this experiment has the advantage for precise theoretical analysis of the discharge process; a spatiotemporal development of the electron and positive ion density in the gap space can be calculated by sloving continuity equations together with Poisson's equation represented in the spheroidal coordinate system. The calculation would provide information on the space charge accumulation process in the gap space and on the photon emission from the r. f. corona, which can be compared with the results of the experiment.

In the present report, basic processes of the r. f. corona discharge are investigated and simulation procedures corresponding to these processes are outlined. The continuity equations for electrons, positive ions and excited molecules, and Poisson's equation are represented with spheroidal coordinates. Taking into account the symmetry of the electrode configuration and experimentally observed appearance of the corona image,[1] an appropriate assumption is made so that the equations used in the simulation become a one dimensional equation. The Phoenical L. P. E. SHASTA algorithm[2,3,4] is used to solve the continuity equation for electrons. This algorithm is modified to be

valid in the spheroidal coordinate system. Boundary conditions are investigated by taking the space charge effect into account. Geometrical factors for the secondary process due to the photoelectric effect at the cathode of the hyperboloidal needle to plane gap are reduced in the spheroidal coordinate system. The simulation procedure is explained by using a flow chart for the computation.

2. Basic processes of the corona discharge development

The development of the corona discharge in nitrogen consists of many primary and secondary processes. In the present simulation, however, the processes are simplified as shown in figure 1. As to the primary processes, only the ionization and the excitation are taken into account in this model. The secondary proceeses consist of the γ_p

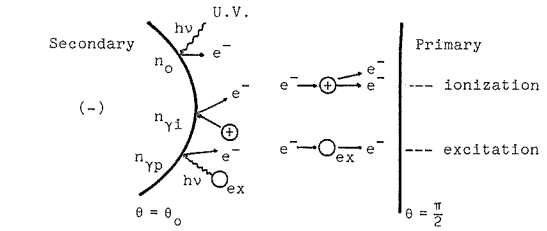

(a) Negative needle electrode.

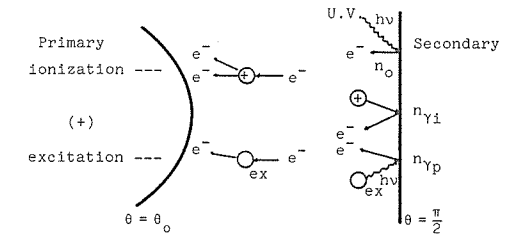

(b) Positive needle electrode.

Figure 1. Main discharge processes.

and γ_i effects which take place on the surface of the upstream electrode for electrons. A preliminary simulation has shown that the development of the corona discharge is mainly controlled by these processes. In this model, the photo-ionization, Penning effect and the γ_m effect are ignored, which would not cause a large discrepancy between the simulation and the experiment. The space charge effect plays a substantial role for the development of the discharge. Both the primary and secondary processes are affected by the space charge effect. Furthermore the accumulation of positive ions due to inoization in front of the needle electrode of negative polarity produces a high field gradient region in the neighbourhood of the needle tip, which provides a non-equilibrium characteristic of the electron swarm[5]. This situation should be taken into account for the simulation.

3. Simulation procedure

The spatio-temporal variations of the electron, positive ion and excited molecule density over the gap space are represented by continuity equations as follows;

$$\text{electron}: \quad \frac{\partial n_e}{\partial t} + \nabla \cdot (n_e \bar{w}_e) = \alpha n_e \bar{w}_e \cdot \frac{\bar{E}}{E} \tag{1a}$$

$$\text{positive ion}: \quad \frac{\partial n_p}{\partial t} - \nabla \cdot (n_e \bar{w}_p) = \alpha n_e \bar{w}_e \cdot \frac{\bar{E}}{E} \tag{1b}$$

$$\text{excited molecules}: \quad \frac{\partial n_{ex}^c}{\partial t} = \alpha_{ex}^{\gamma c} n_e \bar{w}_e \cdot \frac{\bar{E}}{E} - \frac{1}{\tau_{ex}^{\gamma c}} n_{ex}^{\gamma c} \tag{1c}$$

where $\bar{w}_e \cdot \bar{E}$ is the scalar product of the vector $\bar{w}_e$ and $\bar{E}$ and swarm parameters are

α ; ionization coefficient,

α_{ex}^c ; excitation coefficient for the state $C^3\Pi_u$,

α_{ex}^{γ} ; excitation coefficient for the state which is responsible for the γ_p effect,

τ_{ex}^c ; effective life time of the excited state $C^3\Pi_u$,

τ_{ex} ; effective life time of the state which is related to the γ_p effect,

$\bar{w}_e$; electron drift velocity,

$\bar{w}_p$; positive ion drift velocity.

These equations (1a)~(1c) can be solved with the boundary conditions.

For the negative needle electrode,

$$n_e(r_c, t) = n_o(r_c) + n_{\gamma_p}(r_c, t) + n_{\gamma_i}(r_c, t) \text{ at the needle and}$$

$$n_p(r_d, t) = 0 \text{ at the plane,}$$

where r_c and r_d are respectively the position of the upstream and down stream electrode, and n_{γ_p} and n_{γ_i} are the electron densities released from the upstream electrode by the γ_p and γ_i effect, respectively.

For the positive needle electrode,

$$n_e(r_d, t) = n_o(r_d) + n_{\gamma_p}(r_d, t) + n_{\gamma_i}(r_d, t) \text{ at the plane and}$$

$$n_p(r_c, t) = 0 \text{ at the needle.}$$

The swarm parameters used in the continuity equations are functions of the electric field strength. Therefore, they are obtained by using the value of the local field which is the sum of the space charge field and the applied field. For that purpose, the equations (1a)~(1c) must be calculated together with Poisson's equation

$$\nabla \cdot \bar{E} = \frac{e\rho}{\varepsilon_o} \tag{2}$$

where $\rho = n_p - n_e$ is the net charge density.

4. Continuity equations in the spheroidal coordinate system

4. 1. The gap configuration.

The hyperboloidal needle to plane gap configuration is represented by the spheroidal coordinates (η, θ, ϕ) which are related to the Cartesian coordinates (x, y, z) by

the transformation equations

$$x=a\ \cosh\eta\ \cos\theta,\ y=a\ \sinh\eta\ \sin\theta\ \cos\phi \text{ and } z=a\ \sinh\eta\ \sin\theta\ \cos\phi. \quad (3)$$

Combination of the transformation equations with a constant $\theta=\theta_0$ yields

$$\frac{x^2}{a^2\cos^2\theta_0}-\frac{y^2+z^2}{a^2\sin^2\theta_0}=1 \quad (4)$$

This is the standard equation of a hyperbora. Figure 2 shows the geometry of the

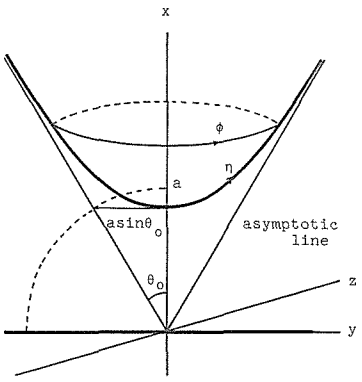

Figure 2. Hyperboloidal needle to plane gap in the spherodial coordinate system.

hyperboloidal needle to plane gap in the spheroidal coordinate system. The needle and plane electrode surfaces correspond to the surfaces represented by equation (4) with $\theta=\theta_0$ and $\theta=\pi/2$, respectively. The parameter a is related to the curvature radius of the needle tip, r_0, and the needle to plane spacing d. The curvature radius of a curved surface is represented as

$$r_0=\left[\left(\frac{dx}{d\eta}\right)^2+\left(\frac{dy}{d\eta}\right)^2\right]^{\frac{3}{2}}\Big/\left|\frac{d^2y}{d\eta^2}\frac{dx}{d\eta}-\frac{d^2x}{d\eta^2}\frac{dy}{d\eta}\right|$$

Using the transformation equations,

$$r_0=\frac{(a^2\cosh^2\eta-a^2\cos^2\theta_0)^{\frac{3}{2}}}{a^2\sin\theta_0\cos\theta_0}$$

At the tip of the needle, $\eta=0$,

$$r_0=\frac{a^2}{a\ \cos\theta_0}-a\ \cos\theta_0=\frac{a^2}{d}-d$$

where $d=a\ \cos\theta_0$.

4. 2. Continuity equations

The continuity equation for electrons is rewritten using the spheroidal coordinates. The second term of equation (1a) is

$$\nabla\cdot(n_e\bar{w}_e)=\frac{1}{h_1h_2h_3}\left[\frac{\partial}{\partial\eta}(h_2h_3n_ew_e)+\frac{\partial}{\partial\theta}(h_3h_1n_ew_e)+\frac{\partial}{\partial\phi}(h_1h_2n_ew_e)\right],$$

where

$$h_1=\left[\left(\frac{\partial x}{\partial \eta}\right)^2+\left(\frac{\partial y}{\partial \eta}\right)^2+\left(\frac{\partial z}{\partial \eta}\right)^2\right]^{\frac{1}{2}},\quad h_2=\left[\left(\frac{\partial x}{\partial \theta}\right)^2+\left(\frac{\partial y}{\partial \theta}\right)^2+\left(\frac{\partial z}{\partial \theta}\right)^2\right]^{\frac{1}{2}}$$

and $$h_3=\left[\left(\frac{\partial x}{\partial \phi}\right)^2+\left(\frac{\partial y}{\partial \phi}\right)^2+\left(\frac{\partial z}{\partial \phi}\right)^2\right]^{\frac{1}{2}}$$

Using the transformation equations,

$$h_1=h_2=a(\sinh^2\eta+\sin^2\theta)^{\frac{1}{2}} \text{ and } h_3=a\ \sinh\eta\ \sin\theta.$$

Considering the symmetry of the gap configuration as shown in figure 2 and observed corona images which are expanded to the η direction[1], assumptions are made as follows;

$$\frac{\partial n_e}{\partial \phi}=0,\ E\phi=E\eta=0 \text{ and } w_{e\phi}=w_{e\eta}=0.$$

Under these assumptions, equation (1a) becomes one dimensional equation with a parameter η,

$$\frac{\partial n_e(\eta,\ \theta,\ t)}{\partial t}=\alpha\ w_{e\theta}n_e-\frac{1}{h_1h_2h_3}\frac{\partial}{\partial \theta}(h_3h_1n_ew_{e\theta}(\eta,\ \theta,\ t)) \tag{5}$$

The precise expression of the second term of equation (5) is

$$\frac{1}{a(\sinh^2\eta+\sin^2\theta)\sin\theta}\frac{\partial}{\partial \theta}\left[(\sinh^2\eta+\sin^2\theta)^{\frac{1}{2}}\ \sin\theta n_eW_{e\theta}\right]$$

For simplicity, equation (5) is rewritten as

$$\frac{\partial n_e}{\partial t}=S-\frac{1}{A_{123}}\frac{\partial}{\partial \theta}(A_{31}n_ew_{e\theta}).$$

This equation can be solved numerically by using the flux corrected transport (F. C. T.) method with the Phoenical L. P. E. SHASTA algorithm.

4. 3. Phoenical SHASTA algorithm

The F. C. T. method has been developed by Boris and Book[2,3] and been adopted for a simulation of the corona discharge development by Morrow[4]. In the present report, this method is modified to be valid in the spheroidal coordinate system. A transport and diffused solution on of equation (5), N_j^1, at the grid position j and the time step $t_1=t_o+\delta t$ is

$$N_j^1=N_j^0-\frac{1}{2}\left[\frac{A_{j+\frac{1}{2}}}{A_j}\frac{\delta x_{j+\frac{1}{2}}}{\delta x_j}\varepsilon_{j+\frac{1}{2}}(N_{j+1}^0+N_j^0)-\frac{A_{j-\frac{1}{2}}}{A_j}\frac{\delta x_{j-\frac{1}{2}}}{\delta x_j}\varepsilon_{j-\frac{1}{2}}(N_j^0-N_{j-1}^0)\right]$$

$$+\frac{A_{j+\frac{1}{2}}}{A_j}\frac{\delta x_{j+\frac{1}{2}}}{\delta x_j}\nu_{j+\frac{1}{2}}(N_{j+1}^0-N_j^0)-\frac{A_{j-\frac{1}{2}}}{A_j}\frac{\delta x_{j-\frac{1}{2}}}{\delta x_j}\nu_{j-\frac{1}{2}}(N_j^0-N_{j-1}^0)$$

with

$$\varepsilon_{j+\frac{1}{2}}=w_{j+\frac{1}{2}}\frac{\delta t}{x_{j+\frac{1}{2}}} \text{ and } \nu_{j+\frac{1}{2}}=\frac{1}{6}+\frac{1}{3}\varepsilon_{j+\frac{1}{2}}^2,$$

where $w_{j+\frac{1}{2}}$ is the electron flow velocity at the half way between grid points j and j+1. $\delta x_{j+\frac{1}{2}}=X_{j+1}-x_j$ is a mesh spacing and $\delta x_j=(\delta x_{j+\frac{1}{2}}+\delta x_{j-\frac{1}{2}})\frac{1}{2}$. A_j and $A_{j+\frac{1}{2}}$ are surface elements at the grid points x_j and $x_j+\delta x_{j+}$, respectively.

in the spheroidal coordinate system, $\delta x_{j+\frac{1}{2}} = a(\sinh^2\eta + \sin^2\theta_j)^{\frac{1}{2}}\delta\theta$ and $A_j = a^2\sinh\eta\ \sin\theta_j (\sinh^2\eta + \sin^2\theta_j)^{\frac{1}{2}}$.

The anti-diffusive fluxes are represented as

$$\Phi_{j+\frac{1}{2}} = \mu_{j+\frac{1}{2}} \frac{A_{j+\frac{1}{2}}}{A_j} \frac{\delta x_{j+\frac{1}{2}}}{\delta x_j} \left\{ N^1_{j+1} - N^1_j + \frac{1}{6}\left[-\frac{A_{j+\frac{3}{2}}}{A_{j+1}} \frac{\delta x_{j+\frac{3}{2}}}{\delta x_{j+1}} (N^0_{j+2} - N^0_{j+1}) \right.\right.$$

$$\left.\left. + \frac{A_{j+\frac{1}{2}}}{A_{j+1}} \frac{\delta x_{j+\frac{1}{2}}}{\delta x_{j+1}} (N^0_{j+1} - N^0_j) + \frac{A_{j+\frac{1}{2}}}{A_j} \frac{\delta x_{j+\frac{1}{2}}}{\delta x_j} (N^0_{j+1} - N^0_j) - \frac{A_{j-\frac{1}{2}}}{A_j} \frac{\delta x_{j-\frac{1}{2}}}{\delta x_j} (N^0_j - N^0_{j-1}) \right] \right\}$$

and

$$\Phi_{j-\frac{1}{2}} = \mu_{j-\frac{1}{2}} \frac{A_{j-\frac{1}{2}}}{A_j} \frac{\delta x_{j-\frac{1}{2}}}{\delta x_j} \left\{ N^1_j - N^1_{j-1} + \frac{1}{6}\left[-\frac{A_{j+\frac{1}{2}}}{A_j} \frac{\delta x_{j+\frac{1}{2}}}{\delta x_j} (N^0_{j+1} - N^0_j) \right.\right.$$

$$\left.\left. + \frac{A_{j-\frac{1}{2}}}{A_j} \frac{\delta x_{j-\frac{1}{2}}}{\delta x_j} (N^0_j - N^0_{j-1}) + \frac{A_{j-\frac{1}{2}}}{A_{j-1}} \frac{\delta x_{j-\frac{1}{2}}}{\delta x_{j-1}} (N^0_j - N^0_{j-1}) - \frac{A_{j-\frac{3}{2}}}{A_{j-1}} \frac{\delta x_{j-\frac{3}{2}}}{\delta x_{j-1}} (N^0_{j-1} - N^0_{j-2}) \right] \right\}$$

where

$$\mu_{j+\frac{1}{2}} = \frac{1}{6}(1 - \varepsilon^2_{j+\frac{1}{2}}) \cdot$$

Using the limiting criteria given by Zalesak[14], corrected anti-diffusive fluxes, $\bar{\Phi}$, are obtained. Then, the value of the update density due to transport is

$$\bar{N}^1_j = N^1_j - \bar{\Phi}_{j+\frac{1}{2}} + \bar{\Phi}_{j-\frac{1}{2}}$$

The source term of equation (5) is written in a form with second order accuracy as

$$S^{1/2}_j = \frac{1}{2}\alpha^{1/2}_j w^{1/2}_{ej} (\bar{N}^1_j + N^0_j + \frac{1}{2}\alpha^0_j w^0_{ej} N^0_j \delta t),$$

where the suffix 1/2 refers to half the time step.

Thus, the required solution of equation at $t_1 = t_0 + \delta t$ is

$$\bar{N}^{1\prime}_j = \bar{N}^1_j + S^{1/2}_j \delta t.$$

The positive ion density n_p is calculated by using equation (1b) and the net charge density is obtained with relation $\rho = n_p - n_e$. However, there is another method to calculate the net charge density, which is more stable for numerical calculations. Combining equation (1a) and (1b), the continuity equation for the net charge density is

$$\frac{\partial \rho}{\partial t} = \frac{\partial}{\partial t}(n_p - n_e) = \nabla \cdot (n_e \bar{w}_e + n_p \bar{w}_p).$$

In the spheroidal coordinate system,

$$\frac{\partial \rho}{\partial t} = \frac{1}{A_{123}} \frac{\partial}{\partial \theta} A_{31} (n_e w_{e\theta} + n_p w_{p\theta}). \tag{7}$$

This equation can be calculated numerically using the Phienical SHASTA algorithm. Then n_p is obtained with the relation $n_p = \rho + n$.

4. 4. Poisson's equation

In the spheroidal coordinate system, equation (2) is represented as

$$\frac{1}{A_{123}}\left[\frac{\partial}{\partial\eta}(A_{23}E_\eta)+\frac{\partial}{\partial\theta}(A_{31}E_\theta)+\frac{\partial}{\partial\theta}(A_{12}E_\phi)\right]=\frac{e\rho}{\varepsilon_0}$$

Neglecting the E_η and E_ϕ according to the assumption in the previous section,

$$\frac{1}{A_{123}}\frac{\partial}{\partial\theta}(h_3h_1E_\theta)=\frac{e\rho}{\varepsilon_0}$$

The detailed expression of this equation is

$$\frac{1}{a(\sinh^2\eta+\sin^2\theta)\sin\theta}\frac{\partial}{\partial\theta}\left[(\sinh^2\eta+\sin^2\theta)^{\frac{1}{2}}\sin\theta E_\theta\right]=\frac{e\rho}{\varepsilon_0} \tag{8}$$

a solution of equation (8) is

$$E_\theta=\frac{1}{(\sinh^2\eta+\sin^2\theta)^{\frac{1}{2}}\sin\theta}\left[\int_{\theta_0}^{\theta}\frac{ae\rho}{e_0}(\sinh^2\eta+\sin^2\theta')\sin\theta'd\theta'+C\right]$$

The integral constant C is obtained by the relation

$$V_a=-\int_{\theta_0}^{\frac{\pi}{2}}\bar{E}\cdot d\bar{l}$$

where V_a is an applied potential between the electrodes and $\bar{l}$ is the arc length along the field direction. For the negative needle electrode,

$$V_a=-\int_{\theta_0}^{\frac{\pi}{2}}E_\theta h_2 d\theta=-\int_{\theta_0}^{\frac{\pi}{2}}a(\sinh^2\eta+\sin^2\theta)^{\frac{1}{2}}E_\theta d\theta$$

Then the solution is written as

$$E_\theta=\frac{V_a}{a(\sinh^2\eta+\sin^2\theta)^{\frac{1}{2}}\sin\theta\log\left(\tan\frac{\theta_0}{2}\right)}-$$

$$\frac{1}{(\sinh^2\eta+\sin^2\theta)^{\frac{1}{2}}\sin\theta\log\left(\tan\left(\frac{\theta_0}{2}\right)\right)}\int_{\theta_0}^{\pi}\log(\tan(\theta/2))\frac{ae\rho}{\varepsilon_0}(\sinh^2\eta+\sin^2\theta)\sin\theta d\theta$$

$$+\frac{1}{(\sinh^2\eta+\sin^2\theta)^{\frac{1}{2}}\sin\theta}\int_{\theta_0}^{\theta}\frac{ae\rho}{\varepsilon_0}(\sinh^2\eta+\sin^2\theta')\sin\theta'\ d\theta'$$

For simplicity, this formula is rewritten as

$$E_\theta=E0-ES1+ES2,$$

where E0 is the electric field without space charge. It is noted that E0 is negative because log $(\tan(\theta_0/2))$ is negative for $\theta_0<\frac{\pi}{2}$.

For the positive needle electrode,

$$V_a=-\int_{\frac{\pi}{2}}^{\theta_0}E_\theta h_2 d\theta\cdot$$

Then $E_\theta=-E0-ES1+ES2$.

5. Swarm parameters

The swarm parameters such as α, α_{ex}, w_e and w_p in nitrogen have been measured by many researchers as a function of the reduced electric field E/p. These values can

be represented by appropriate functions of E/p=Z;

$$\alpha/p=7.56\ \exp(-272/|Z|) \qquad (1/\text{cm Torr})$$

$$\alpha^{c}_{ex}/p=6.8\ \exp(-138.6/|Z|) \qquad (1/\text{cm Torr})$$

$$w_e=3.1\text{x}10^5 Z \qquad (\text{cm/sec})$$

$$w_p=\begin{cases}2.0\text{x}10^3(1-4\text{x}10^{-3}Z)Z & Z<80\\ 1.25\text{x}10^4 Z^{1/2}-2.4\text{x}10^5 Z & Z\geq 80\end{cases} \qquad (\text{cm/sec})$$

The function for α/p agrees with the measured E/p dependence of α/p by Masch[6], Frommhold[7], Kontoleon[8] and Williams and Haydon[9]. The data for τ^{c}_{ex}/p are taken from Legler[10]. w_e is from Tholl[11] and Frommhold[7]. w_p is from Dahlquist[12] and Saporoschenko[13]. The effective life time of the $C^3\Pi_u$ state, τ^{c}_{ex}, is obtained by the relation

$$1/\tau^{c}_{ex}=1/\tau^{c}_{0}(1+p/p_q),$$

where τ^{c}_{0} (40 ns) is the radiative life time and p_q (60 Torr) is the quenching pressure[10].

It should be noted that the swarm parameters were measured under equilibrium conditions of the electron and ion swarm. Under the field conditions with a high field gradient, however, the electron swarm is not always in equilibrium[5]. For the present case, the high field gradient region may be produced in the neighbourhood of the sharp needle tip. The space charge distribution may also give rise to a high field gradient in the gap space. Therefore, it is necessary to obtain non-equilibrium values of the swarm parameter which correspond to the present situation. For that purpose, it is useful to use a quasi-microscopic calculation method for the ionization coefficient[5,15]. Nonequilibrium values of the ionization coefficient can be obtained by solving the equation

$$\frac{d\alpha}{dx}+\alpha^2+pk\xi\alpha-p(a+\frac{2ak\xi^2}{E/p})\exp(-k\xi^2/E/p)E=0, \qquad (7)$$

where p and ξ are the gas pressure and the inelasic or ionization collision threshold energy, respectively. K and a are the total inelastic and ionization collision efficiencies per unit energy, respectively.

6. Boundary conditions

6. 1. Negative needle electrode

As described in section 2, the needle and plane electrodes are the upstream electrode for electrons and positive ions, respectively. Then, the boundary conditions are

$$n_e(\theta_0,\ t)=n_0+n_{\gamma i}(\theta_0,\ t)+n_{\gamma p}(\theta_0,\ 0)\text{and}\ n_p(\frac{\pi}{2},\ t)=0.$$

n_0 is the electron density released from the needle electrode by an external U. V. irradiation. $n_{\gamma i}(\theta_0,\ t)$ is the electron density produced at the needle surface by the ion impact to the needle electrode (γ_i effect) and given as

$$n_{\gamma i}(\theta_0,\ t)=\Gamma_i n_p(\theta_0,\ t)w_{p\theta}(\theta_0,\ t)/w_{e\theta}(\theta_0,\ t),$$

where $\Gamma_1(10^{-4}\sim10^{-5})$ is the efficiency of this effect which depends on the electrode material and surface condition. $n_{\gamma p}(\theta_0, t)$ is the electron density released from the needle electrode by photons from avalanches (γ_p effect). The excited molecules n_{ex} may emit photons which have an energy high enough to release electrons from the needle surface. The spatial distribution of the n_{ex} is obtained by solving the continuity equation

$$\frac{\partial n_{ex}}{\partial t} = \alpha^{\gamma}_{ex}\, n_e\, w_{e\theta} - \frac{1}{\tau^{\gamma}_{ex}} n^{\gamma}_{ex} \tag{10}$$

In nitrogen gas, it is very difficult to identify the excited state which is responsible for the γ_p effect. It can be considered, however, that the high energy photon emission may come from an excited state which is located in the neighbourhood of the ionization threshold. Therefore, it may be reasonable to assume that the energy dependence of the α^{γ}_{ex} is similar to that of the ionization coefficient α and the life time τ_{ex} is as short as a couple of nanoseconds. Solving equation (10) at $t=t_0+\delta t$,

$$n^{\gamma}_{ex}(\eta, \theta, t_0+t) = -\frac{\delta t}{\tau^{\gamma}_{ex}}\left[\int_{t_0}^{t_0+t} \exp\left(\frac{t'-t_0}{\tau^{\gamma}_{ex}}\right)\alpha^{\gamma}_{ex} n_e w_{e\theta} dt' + n^{\gamma}_{ex}(t_0)\right]$$

The photon flux density at the position $(\eta_0, \theta_0, \phi_0)$ on the needle surface is

$$\frac{d}{dt} n_{ph}(\eta_0, \theta_0, \phi_0, t) = \frac{1}{\tau^{\gamma}_0}\iiint g(\eta_0, \theta_0, \phi_0; \eta, \theta, \phi) n^{\gamma}_{ex}(\eta, \theta, \phi) h_1 h_2 h_3 d\eta d\theta d\phi.$$

g is the geometrical factor which is given as

$$g = \frac{1}{4\pi}\frac{\cos\theta_a}{R} = \frac{\bar{n}\cdot\bar{R}}{4\pi|R|^3} \qquad \text{(see figure 3)} \tag{11}$$

where $\bar{n}$ is the unit normal vector at $(\eta_0, \theta_0, \phi_0,)$ on the needle surface and $\bar{R}$ is the

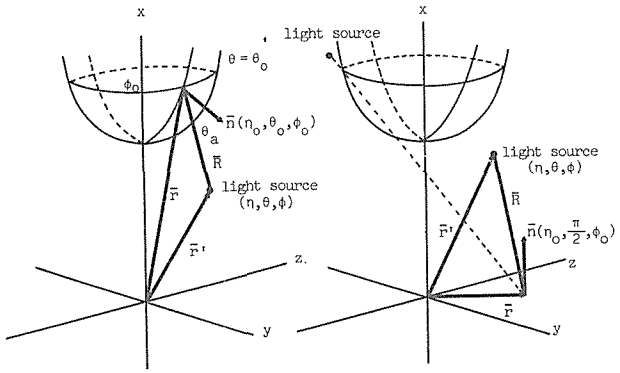

Figure 3. Geometrical factor for the γ_p process.

distance between a photon source (η, θ, ϕ) and the position $(\eta_0, \theta_0, \phi_0)$. The unit normal vector $\bar{n}$ is obtained by the relation

$$\bar{n} = \left(\frac{\partial \bar{r}}{\partial \phi} \times \frac{\partial \bar{r}}{\partial \eta}\right) \Big/ \left|\frac{\partial \bar{r}}{\partial \phi} \times \frac{\partial \bar{r}}{\partial \eta}\right| \text{ at } (\eta_0, \theta_0, \phi_0).$$

When the numerator of equation (11) is negative, $g=0$.

Then,

$$n_{\gamma p}(\eta_0,\ \theta_0,\ t)=\Gamma_p\frac{1}{w_{e\theta}(\eta_0,\ \theta_0,\ t)}\frac{dn_{ph}(\eta_0,\ \theta_0,\ t)}{dt},$$

where Γ_p is the photoelectric efficiency of the electrode surface. The value of $\Gamma_p(10^{-3}\sim10^{-4})$ depends on the electrode material and surface condition.

6. 2. Positive needle electrode

In this case, the needle and plane electrode are the upstream electrodes for ions and electrons, respectively. Then, the boundary conditions are

$n_p(\theta_0,\ t)=0$ at the needle and

$$n_e\left(\frac{\pi}{2},\ t\right)=n_0+n_{\gamma i}\left(\frac{\pi}{2},\ t\right)+n_{\gamma p}\left(\frac{\pi}{2},\ t\right)\ \text{at the plane.}$$

$n_{\gamma i}$ is given as

$$n_{\gamma i}=\Gamma_i n_p\left(\frac{\pi}{2},\ t\right)w_{p\theta}\left(\frac{\pi}{2},\ t\right)/w_{e\theta}\left(\frac{\pi}{2},\ t\right).$$

For the γ_p effect,

$$n_{\gamma p}=\Gamma_p\frac{1}{w_{e\theta}\left(\frac{\pi}{2},t\right)}\frac{1}{\tau_0^{\gamma}}\iiint g(\eta_0,\ \frac{\pi}{2},\ \phi_0\,;\ \eta,\ \theta,\ \phi)n_{ex}^{\gamma}(\eta,\ \theta,\ \phi)h_1h_2h_3d\eta d\theta d\phi$$

As shown in figure 3, it is noted that some portions of photons produced in the neighbourhood of the side surface of the needle electrode at a large η can not reach a position on the plane surface. However, this effect on the γ_p process may be small because the $n_{\gamma p}(n_0,\ \frac{\pi}{2},\ t)$ decreases sharply with increasing η.

6. 3. For the case with a high space charge density

When the space charge field become intense, the boundary conditions are changed at both the negative and positive needle electrodes. As shown in figures 4 (a) and (b), a prelinminary calculation has shown that both the needle and plane electrodes are

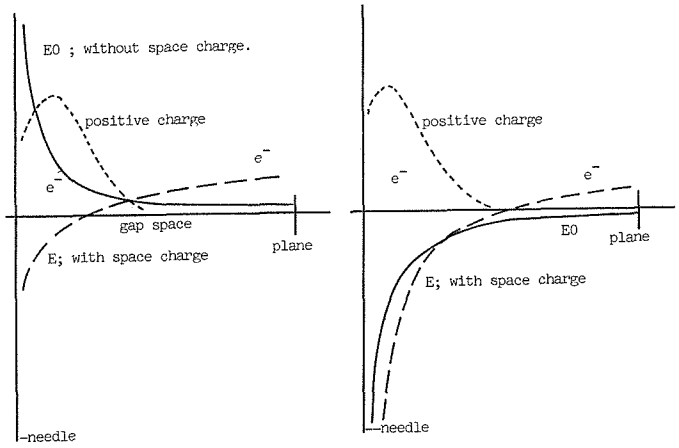

Figure 4. Spactial variation of the electric field with a high space charge density.

the upstream electrode. In this case, the boundary conditions are

$$n_e(\theta_0,\ t)=n_0+n_{\gamma i}(\theta_0,\ 0)+n_{\gamma p}(\theta_0,\ t),\ n_p(\theta_0,\ t)=0,$$

$$n_e(\frac{\pi}{2},\ t)=n_0+n_{\gamma i}(\frac{\pi}{2},\ t)+n_{\gamma p}(\frac{\pi}{2},\ t) \text{ and } n_p(\frac{\pi}{2},\ t)=0.$$

7. Flow chart for the computation

Figure 5 shows a basic flow chart of the simulation. Each step is explained as follows.

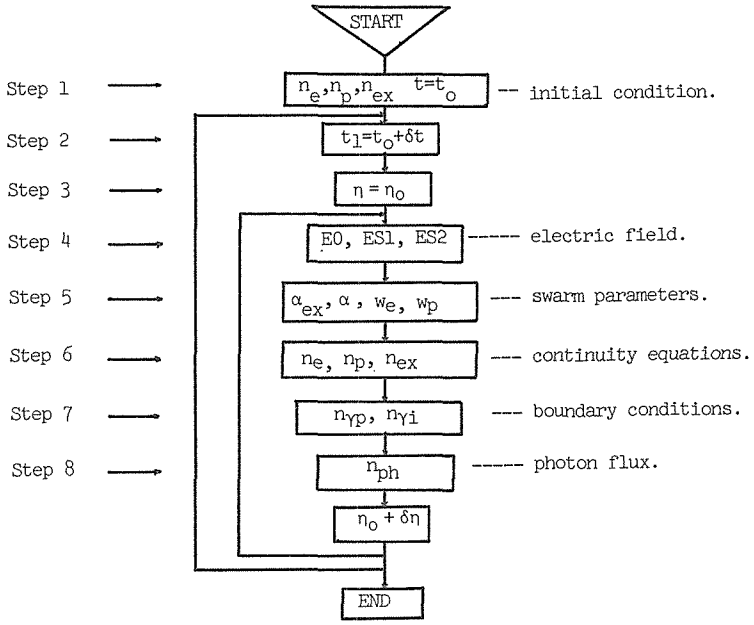

Figure 5. Flow chart for computation.

Step 1: The initial conditions are given by $n_e(\eta,\ \theta,\ t_0)=0$, except $n_e(\eta,\ \theta_0,\ t_0)=n_0$ for the negative needle and $n_e(\eta,\ \frac{\pi}{2},\ t_0)=n_0$ for the positive needle electrode. For the ion and excited molecule densities, $n_p(\eta,\ \theta,\ t_0)=0$, $n^c_{ex}(\mu,\ \theta,\ t_0)=0$ and $n_{ex}(\eta,\ \theta,\ t_0)=0$.

Step 2: The time increment δt should be taken small so that the Courant-Fredrichs-Lewy condition is fulfilled. For the present algorithm,

$$\delta t<\frac{\delta\theta\ h_2}{2w_{e\theta}^{max}} \tag{12}$$

where $w_{e\theta}^{max}$ is the maximun value of $w_{e\theta}$ in the gap space.

Step 3: The calculations are carried out along the θ axis with a different value of η which works as a parameter. The range of the value of η is taken from $\eta=0$ (along the symmetry axis of the electrode system) to $\eta=\eta_{max}$ with a small increment $\delta\eta$. The η_{max} is given by taking into account the appearance of the observed corona image.

Step 4: The time varying applied field V_a (t) is given as

$$V_a(t)=F(t)\sin\omega t,$$

where $\omega=2\pi f$ is the angular frequency of the r. f. voltage and F(t) is a function which represents the r. f. pulse envelope. For example, $F(t)=(1-\exp(-t/T))\cdot V_a$, where T is a rising time constant of the pulse and V_0 is the r. f. peak voltage. Then, the electric field without space charge is written as

$$E0=\frac{F(t)\sin\omega t}{a(\sinh^2\eta+\sin^2\theta)^{\frac{1}{2}}\sin\theta\log\left(\tan\left(\frac{\theta_0}{2}\right)\right)}$$

Step 5: The swarm parameters are obtained by using the absolute value of the reduced electric field $|E/p|=|Z|$. However, the sign of w_e and w_p should be determined by considering the direction of the electric field at each position along the θ axis. The continuity equations (1a) and (1b) indicate that w_e is positive when the electron at a certain position in the gap moves towards the needle electrode. In this situation, the positive ion moves towards the plane electrode and then w_p is also positive. In the spheroidal coordinate system, however, the signs of w_e and w_p are opposite to those represented in the Cartesian coordinate system. For example,

$$w_{e\theta}=\frac{1}{h_2}\frac{\partial x}{\partial\theta}w_{ex}+\frac{1}{h_2}\frac{\partial y}{\partial\theta}w_{ey}+\frac{1}{h_2}\frac{\partial z}{\partial\theta}w_{ez}.$$

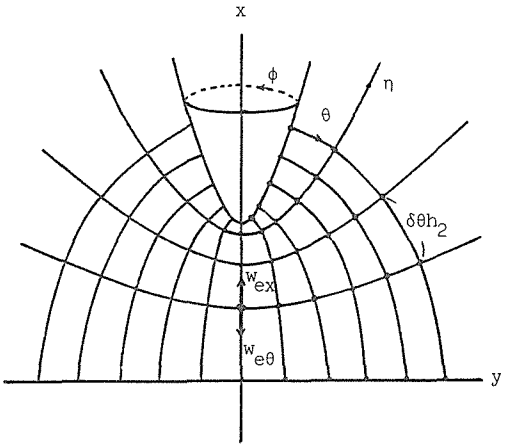

Figure 6. Mesh point in the spheroidal coordinate system.

Along the symmetry axis of the electrode system, $w_{e\theta}=-\sin\theta w_{ex}/\sin\theta=-w_{ex}$ (see figure 6). Then $w_{e\theta}$ is negative when electrons move towards the needle electrode.

Step 6: The continuity equations are solved at each mesh point on the θ axis with

a small increment $\delta\theta$. The amount of $\delta\theta$ should be set as small as to have the relation (12) satisfied. Fortunately, the arc length $\delta\theta h_2$ becomes small automatically with a uniform mesh of $\delta\theta$ in the neighbourhood of the needle electrode where the electron drift velocity is large. In the course of the calculation, n_e and n_p is maintained to be positive or zero so that a calculated negative density is set at equal zero. At the boundary, the calculation is carried out by using upwind differencing.

Step 7: In order to calculate $n_{\gamma p}$ and $n_{\gamma i}$, the value of the unknown parameters such as Γ_p, Γ_i, τ_{ex} and τ_0 should be set appropriately. These parameters may work in such a way as to adjust parameters to fit the calculation with the experiment.

Step 8: The emission from the excited molecule of the $C^3\Pi_u$ state can be calculated as a photon flux

$$\psi_{ph}^c = \frac{\partial n_{ph}}{\partial t} = n_{ex}^c / \tau_0^c.$$

The calculated spatial variation of log ψ_{ph}^c can be compared with photographs of the r. f. corona images.

These steps are repeated until t reaches the required time. A preliminary calculation shows that for 4000 times iteration of this cycle takes about 30 seconds of the C. P. U. time by using HITAC 280.

Acknowledgments

The authors wish to acknowledge the valuable discussions with Professor S. C. Haydon of The University of New England, Australia, and Dr. R. Morrow of C. S. I. R. O, A. P. D, Australia.

References

1) N. Sato and S. C. Haydon: The 3rd Gaseous Electronics Meeting in Australia Canberra 8-10 th Feb. (1984)
2) J. P. Boris and D. L. Book: J. Comp. Phys. **11** 38-69 (1973)
3) J. P. Boris and D. L. Book: J. Comp. Phys. **20** 397-431 (1976)
4) R. Morrow: J. Comp. Phys. **46** 454-461 (1982)
5) N. Sato and H. Tagashira: submitted to J. Phys. D
6) K. Masch: Archiv. Elektrotechnik **26,** 587 (1932)
7) L. Frommhold: Z. Phys. **160** 554 (1960)
8) N. Kontoleon et al.: J. Phys. D **6** 1237 (1976)
9) S. C. Haydon and O. M. Williams: J. Phys. D **9** 523 (1976)
10) W. Legler: Z. Phys. **173** 169 (1963)
11) H. Tholl: Z. Phys. **178** 183 (1964)
12) J. A. Dahlquist: J. Chem. Phys. **39** 1203 (1963)
13) M. Saporoschenko: Phys. Rev. **139** 352 (1965)
14) S. T. Zalesak: J. Comp. Phys. **31** 335 (1979)

15) L. Friedland: J. Phys. D **7** 2246 (1974)